A Climatology of Midlatitude Continental Clouds from the ARM SGP Central Facility: Part I: Low-Level Cloud Macrophysical, Microphysical, and Radiative Properties

XIQUAN DONG

Department of Atmospheric Sciences, University of North Dakota, Grand Forks, North Dakota

PATRICK MINNIS

Atmospheric Sciences, NASA Langley Research Center, Hampton, Virginia

BAIKE XI

Department of Atmospheric Sciences, University of North Dakota, Grand Forks, North Dakota

(Manuscript received 4 March 2004, in final form 14 October 2004)

ABSTRACT

A record of single-layer and overcast low cloud (stratus) properties has been generated using approximately 4000 h of data collected from January 1997 to December 2002 at the Atmospheric Radiation Measurement (ARM) Southern Great Plains Central Facility (SCF). The cloud properties include liquid-phase and liquid-dominant mixed-phase low cloud macrophysical, microphysical, and radiative properties including cloud-base and -top heights and temperatures, and cloud physical thickness derived from a ground-based radar and lidar pair, and rawinsonde sounding; cloud liquid water path (LWP) and content (LWC), and cloud-droplet effective radius (r_e) and number concentration (N) derived from the macrophysical properties and radiometer data; and cloud optical depth (τ), effective solar transmission (γ), and cloud/top-of-atmosphere albedos ($R_{\rm cldy}/R_{\rm TOA}$) derived from Eppley precision spectral pyranometer measurements. The cloud properties were analyzed in terms of their seasonal, monthly, and hourly variations. In general, more stratus clouds occur during winter and spring than in summer. Cloud-layer altitudes and physical thicknesses were higher and greater in summer than in winter with averaged physical thicknesses of 0.85 and 0.73 km for day and night, respectively. The seasonal variations of LWP, LWC, N, τ, $R_{\rm cldy}$, and $R_{\rm TOA}$ basically follow the same pattern with maxima and minima during winter and summer, respectively. There is no significant variation in mean r_e, however, despite a summertime peak in aerosol loading. Although a considerable degree of variability exists, the 6-yr average values of LWP, LWC, r_e, N, τ, γ, $R_{\rm cldy}$, and $R_{\rm TOA}$ are 151 gm^{-2} (138), 0.245 gm^{-3} (0.268), 8.7 μm (8.5), 213 cm^{-3} (238), 26.8 (24.8), 0.331, 0.672, and 0.563 for daytime (nighttime). A new conceptual model of midlatitude continental low clouds at the ARM SGP site has been developed from this study. The low stratus cloud amount monotonically increases from midnight to early morning (0930 LT), and remains large until around local noon, then declines until 1930 LT when it levels off for the remainder of the night. In the morning, the stratus cloud layer is low, warm, and thick with less LWC, while in the afternoon it is high, cold, and thin with more LWC. Future parts of this series will consider other cloud types and cloud radiative forcing at the ARM SCF.

1. Introduction

Clouds are one of the largest sources of uncertainty in predicting any potential future climate change (Wielicki et al. 1995; Houghton et al. 2001) and have been classified as the highest priority by the U.S. Climate Change Research Initiative (USCCRI 2001; see online at www.climatescience.gov/about/ccri.htm). The importance of cloud-radiative interactions to global climate has been highlighted by many investigators (e.g., Wetherald and Manabe 1988; Mitchell and Ingram 1992; Houghton et al. 2001). The impact of clouds on the Earth's radiation budget mainly depends on cloud amount and height, cloud particle size and shape, and cloud (or ice) water content (Curry et al. 2000; Houghton et al. 2001). Because various climate models have different representations of cloud microphsyical and radiative properties, an intercomparison of 19 general circulation models (GCMs) produced a variety of cloud feedback results, ranging from modest negative to strong positive (Cess et al. 1990). A recent updated comparison by Cess et al. (1996) showed a more narrow

Corresponding author address: Dr. Xiquan Dong, Dept. of Atmospheric Sciences, University of North Dakota, 4149 Campus Road, Box 9006, Grand Forks, ND 58202-9006.
E-mail: dong@aero.und.edu

difference with most models producing modest cloud feedback because they changed their cloud optical properties in the models, such as an improper cloud droplet radius. Much effort has been expended to better understand and parameterize a few cloud types, especially cirrus and marine stratus and stratocumulus. Marine stratus and stratocumulus clouds have been the foci of considerable research that employed models (e.g., Bretherton and Wyant 1997), surface (e.g., Klein and Hartmann 1993), in situ (e.g., Albrecht et al. 1988), and satellite observations (e.g., Minnis et al. 1992). Although most emphasis in the climate community has been on marine stratus/stratocumulus clouds, continental stratus should share some of the same characteristics. To have a long-term record of their behavior, something not easily done over ocean, is of considerable value.

To study the interactions between radiation and clouds of all types, the Department of Energy Atmospheric Radiation Measurement (ARM) program established the ARM Southern Great Plains (SGP) central facility (SCF; 36.6°N, 262.5°E) in 1992 (Stokes and Schwartz 1994; Ackerman and Stokes 2003). In addition to better understanding of clouds and radiation, the ARM program is designed to use long records of surface observations to develop, test, and improve cloud parameterizations in the context of single general circulation model (GCM) grid columns and then to transfer the resulting parameterizations into full three-dimensional GCMs (Randall et al. 1996). To begin the process of evaluating cloud parameterizations and validating satellite retrievals using ARM surface observations, Dong et al. (2000) used ground-based data to generate a database of low-cloud properties for overcast and single-layer cloud events that occurred from November 1996 through November 1998 at the SCF. However, that database, which includes only 2 yr of daytime cloud properties, is insufficient as a statistically reliable climatology and cannot adequately describe the diurnal cycle of continental stratus at the SCF. Since the publication of Dong et al. (2000), we have compiled a more extensive record of single-layer and overcast low cloud macrophysical, microphysical, and radiative properties using data collected for 6 yr at the SCF from January 1997 to December 2002. During this period, the liquid-phase and liquid-dominated mixed-phase low clouds occurred frequently providing many opportunities to retrieve their microphysical and radiative properties using the approach of Dong et al. (1998). The resulting record of cloud properties provides a unique source of instantaneous and climatological information for studying seasonal, monthly, and diurnal variations of the midlatitude continental low cloud properties, evaluating climate and regional forecast model parameterizations, and serving as the ground-truth for satellite validation. As the first part of a series, this paper documents fundamental statistical information about the midlatitude continental low cloud properties at the SCF. It adds an additional 4 yr to the Dong et al. (2000) results and expands the scope from daytime only to include both daytime and nighttime cloud properties. Thus, the diurnal cycles of continental low cloud properties are examined in detail.

2. Data and analysis methods

To obtain more reliable cloud microphysical and radiative property retrievals, the cloudy cases selected in this study are single-layer and overcast low clouds that persist for approximately 2 h at the SCF. The low clouds include mostly continental stratus and stratocumulus, and some shallow cumulus clouds with cloud-base and -top heights less than 3 and 4 km, respectively. Five criteria were established for choosing the conditions under which daytime cloud properties can be estimated. These criteria are (i) only single-layer and overcast low clouds are present as determined from cloud radar observations, (ii) cloud-top altitude Z_{top} is less than 4 km, (iii) the liquid water path LWP is between 20 and 700 g m^{-2}, (iv) the cosine of solar zenith angle (μ_0) is larger than 0.2, and (iv) the range of effective solar transmission (γ) is between 0.08 and 0.7. The physical reasons for using these five criteria are discussed in Dong et al. (2000). For nighttime cloud retrieval criteria, the daytime criteria (i) to (iii) can also be applied, with an additional criterion: the cloud radar reflectivity ranges from -60 to -10 dBZ. These criteria should, in general, correspond to the stratus, stratocumulus, and fog (SSF) category used in the surface observed climatology of Warren et al. (1986). Approximately 2163 h (~26 000 samples at 5-min resolution) of daytime data and 1839 h (~22 000 samples at 5-min resolution) of nighttime data satisfied the above criteria during the 6-yr period.

The datasets (5-min resolution) in this study were collected from direct surface measurements or derived from surface measurements, as well as calculated from the newly developed parameterizations of Dong et al. (1998) and Dong and Mace (2003a). The main surface observations and retrievals, as well as their uncertainties and references used in this study are listed in Table 1. The centerpiece of the cloud instrument array is the millimeter wavelength cloud radar (MMCR; Moran et al. 1998). The MMCR operates at a wavelength of 8 mm in a vertically pointing mode and provides continuous profiles of radar reflectivity from hydrometeors moving through the radar field of view, allowing the identification of clear and cloudy conditions. Cloud-top height (Z_{top}) is derived from MMCR reflectivity profiles and cloud-base height (Z_{base}) is derived from a composite of Belfort laser ceilometer, Micropluse lidar (MPL), and MMCR data (CloudBaseBestEstimate; Clothiaux et al. 2000). Since the laser ceilometer and lidar are sensitive to the second moment of the particle distribution (or the cross-sectional area of the particle) instead of sixth moment like the MMCR, the ceilome-

TABLE 1. Cloud property measurement and retrieval methods used at the ARM SCF.

Cloud parameter	Instruments/methods	Uncertainty	References
Cloud-base height	Ceilometer	8 m	Clothiaux et al. (2000)
Cloud-base hieght	Micropulse lidar	30 m	Clothiaux et al. (2000)
Cloud-top height	Microwave cloud radar	45 m	Clothiaux et al. (2000)
Cloud-base and cloud-top temperatures	Radiosonde sounding	0.2°C	ARM Web site www.arm.gov
Cloud LWP	Microwave radiometer	~20 g m^{-2} for LWP < 200 ~10% for LWP > 200	Dong et al. (2000); Liljegren et al. 2001
Cloud LWC	LWP/cloud thickness		
r_e	Parameterization_1	~10% for daytime	Dong et al. (1998, 2002)
	Parameterization_2	~15% for nighttime	Dong and Mace (2003a)
N	Parameterization_1	~20%–30% for daytime	Dong et al. (1998, 2002)
	Parameterization_2	~30%–40% for nighttime	Dong and Mace (2003a)
τ	Parameterization_1	~5% for daytime	Dong et al. (1998, 2002)
	Parameterization_2	~10% for nighttime	Dong and Mace (2003a)
R_{cldy}, R_{TOA}	Parameterization_1	~5% for daytime	Dong et al. (1998, 2002)
γ	SW↓(cloud)/SW↓(clear)	~5% for daytime	Long and Ackerman (2000)

ter and lidar can provide a more faithful estimate of Z_{base} than MMCR because MMCR often detects precipitation-sized particles below cloud base and false cloud base due to the insect interference of MMCR observations at the SGP site. The ceilometer and lidar signals, however, can be severely attenuated due to absorption by optically thick liquid cloud layers, and these signals can only penetrate through the cloud base about 200 m (Sassen 1991). Therefore, the ceilometer/lidar derived Z_{base} is used as the lowest Z_{base}.

Cloud-base and -top temperatures, T_{base} and T_{top}, respectively, are estimated from a linear temporal interpolation of ARM SCF rawinsonde soundings (~4 times per day) using Z_{base} and Z_{top}. Cloud physical thickness (ΔZ) is simply the difference between Z_{top} and Z_{base}. The LWP is derived from the microwave radiometer brightness temperatures measured at 23.8 and 31.4 GHz using a statistical retrieval method (Liljegren et al. 2001). The up- and down-looking standard Eppley Precision Spectral Pyranometers (PSPs) provide measurements of downward and upward broadband shortwave (0.3–3 μm) fluxes at the surface, respectively. The effective solar transmission γ is the ratio of the measured cloudy downward shortwave flux at the surface to the inferred clear-sky downward shortwave flux that would be recorded by the broadband pyranometer if there were no clouds present (Long and Ackerman 2000).

The daytime microphysical and radiative properties of single-layer and overcast low clouds are calculated using the parameterizations of Dong et al. (1998, hereafter D98). Given a measurement of LWP, the technique of Dong et al. (1997, hereafter D97) uses an iterative approach that varies cloud-droplet effective radius (r_e) in δ2-stream radiative transfer model calculations until the computed effective solar transmission matches the measured value. Optical depth is then computed from the retrieved values of LWP and r_e. The motivation for using γ instead of downward solar flux at the surface is to account for the biases between measured and modeled surface downward solar flux (Kato et al. 1997). The retrieved r_e and cloud albedo were then parameterized as a function of the cloud LWP, γ, and the cosine of the solar zenith angle (μ_0) (D98). It should be mentioned that the application of these parameterizations in this study exceed the original low and upper boundaries as stated in the D98 study. For example, the minimum μ_0 has been extended from 0.4 to 0.2, the maximum LWP from 600 to 700 gm^{-2}, and the lower γ from 0.1 to 0.08. The motivation for expanding the limits of the D98 parameterizations is to use as many cases and samples as possible to enhance the statistics of each parameter. Because they represent a greater range of cases, the statisitics can be more reliably compared with cloud and climate model simulations.

To determine the impact of altering the limits, the cloud microphysical and radiative properties based on the D98 lower and upper limits were computed and found to have values almost identical to those in Table 2 but with about 30% fewer samples. To further test the accuracy of the D98 parameterizations, the D97 retrieval method was applied to 3 months (December 1997–February 1998) of data (~150 h) at the SCF and subsequently compared to the estimates from the D98 parameterizations. Differences between the retrieved and parameterized values were generally within 3%. Another finding from that comparison was that the top-of-atmosphere (TOA) albedo, on average, was about 84% of cloud albedo within 2% variation. Therefore, the TOA albedo can be obtained by multiplying the parameterized cloud albedo by 0.84 in this study. From this 3-month comparison as well as comparisons with aircraft in situ measurements (D98; Dong et al. 2002; Dong and Mace 2003a), the D98 parameterizations, developed from a total of 25 h of ground-based observations of stratus taken in the Azores and Oklahoma, can be extensively applied in the midlatitudes to areas with low surface albedo (~0.2), but not to those with high surface albedo (Dong and Mace 2003b).

The nighttime r_e values are calculated using an em-

TABLE 2. Seasonal and yearly averages, standard deviations, medians, and modes of various cloud parameters derived from the 6-yr ARM SGP dataset

	Winter		Spring		Summer		Autumn		Year	
	Day	Night	Day	Night	Day	Night	Day	Night	Day	Night
C_f	0.180	0.153	0.176	0.130	0.097	0.069	0.179	0.134	0.158	0.128
	0.11	0.06	0.13	0.07	0.14	0.08	0.17	0.11	0.09	0.06
Z_{base}, km	0.77	0.82	0.97	1.0	1.17	1.39	0.94	1.12	0.94	1.0
	0.68	0.68	0.66	0.79	0.71	0.91	0.73	0.91	0.70	0.82
	0.60	0.62	0.82	0.77	1.09	1.25	0.70	0.74	0.74	0.71
	0.3	0.5	0.5	0.5	0.8	0.7	0.5	0.4	0.5	0.5
Z_{top}, km	1.46	1.44	1.89	1.88	2.16	2.24	1.73	1.81	1.79	1.73
	0.80	0.78	0.78	0.81	0.72	0.78	0.86	0.97	0.83	0.88
	1.25	1.25	1.82	1.73	2.09	2.15	1.55	1.58	1.67	1.51
	1.1	1.1	1.3	1.5	1.9	1.9	1.1	0.9	1.1	1.1
ΔZ, km	0.69	0.62	0.94	0.88	1.0	0.85	0.79	0.69	0.85	0.73
	0.57	0.54	0.66	0.66	0.56	0.49	0.60	0.57	0.62	0.59
	0.55	0.46	0.80	0.74	0.89	0.81	0.63	0.52	0.70	0.57
	0.3	0.3	0.3	0.3	0.7	0.7	0.3	0.3	0.3	0.3
T_{base}, K	271.4	271.4	279.6	277.7	289.5	288	281.6	279.6	279.4	276.7
	7.1	7.2	8.5	9.1	5.4	6.7	9.9	7.9	10	9.3
	271.4	270.8	280	277.8	290.1	289.7	282.6	280.4	279.9	276.2
	272.5	272.5	277.7	277.5	292.5	292.5	285	282.5	280	272.5
T_{top}, K	271.1	271.1	277.3	276	285.4	284.6	279.8	278.3	277.5	275.5
	8.8	9.0	10.1	10.8	6.6	7.1	9.5	8.5	10.3	10.3
	271.7	272	278.4	276.6	286.5	285.7	281.3	279.8	278.8	275.8
	272	270	277.5	272.5	287.5	287.5	282.5	282.5	282.5	272.5
LWP, gm^{-2}	141.1	130.4	160	158.9	123	112.3	165.3	135.5	150.7	137.9
	108	106	135	135	115	110	139	118	127	119
	113.6	104.5	115.3	116.9	82.9	80.1	119.7	99.2	109.7	103.4
	75	75	75	75	75	75	75	75	75	75
LWC, gm^{-3}	0.282	0.296	0.24	0.250	0.16	0.18	0.27	0.28	0.25	0.268
	0.46	0.36	0.21	0.22	0.17	0.20	0.25	0.23	0.30	0.28
	0.25	0.259	0.19	0.21	0.11	0.126	0.22	0.241	0.20	0.232
	0.22	0.19	0.075	0.1	0.075	0.075	0.15	0.15	0.075	0.1
r_e, μm	8.4	8.6	8.7	8.6	8.9	8.1	9.0	8.4	8.7	8.5
	3.2	3.4	3.0	2.8	3.2	2.0	3.3	2.9	3.2	3.0
	7.8	8.0	8.2	8.1	8.4	8.0	8.4	7.8	8.2	8.0
	7.0	7.5	7.5	7.5	8.0	7.5	7.5	7.0	7.5	7.5
N, cm^{-3}	281	265	200	219	128	159	217	249	213	238
	296	269	245	257	188	211	253	267	258	263
	174	171	111	128	59	88	126	159	117	147
	50	50	25	75	25	25	25	50	25	25
τ	26.4	23.0	28.5	28.3	22.1	21.4	27.9	24.7	26.8	24.8
	16.9	15.4	21.6	22.1	19.8	19.6	19.7	18.8	19.9	18.9
	22.7	19.6	22.3	22.0	15.3	16.6	22.4	19.7	21.2	20.0
	7.5	15	7.5	12.5	7.5	12.5	12.5	12.5	7.5	12.5
γ	0.297		0.327		0.437		0.303		0.331	
	0.19		0.21		0.24		0.20		0.21	
	0.246		0.276		0.401		0.262		0.280	
	0.175		0.175		0.375		0.125		0.175	
R_{cldy}	0.702		0.668		0.605		0.686		0.672	
	0.13		0.13		0.15		0.13		0.14	
	0.736		0.695		0.607		0.710		0.697	
	0.825		0.775		0.625		0.825		0.775	
R_{TOA}	0.588		0.560		0.507		0.575		0.563	
	0.11		0.11		0.12		0.11		0.12	
	0.617		0.582		0.509		0.595		0.584	
	0.675		0.625		0.525		0.675		0.675	

pirical relationship between effective radius and radar reflectivity based on both theory and the daytime retrievals (Dong and Mace 2003a). Then, the nighttime cloud-droplet number concentration and optical depth are calculated using the same method as its daytime counterpart. The empirical relationship was derived from only a total of 36 h of surface data, and validated by 10 h of aircraft in situ measurements during the March 2000 ARM cloud field experiment. Therefore, this relationship may be changed and should be used with caution for case studies. For statistical studies, it should produce a statistical result similar to its daytime counterpart, which has been proven in Table 2, and Figs. 4 and 5.

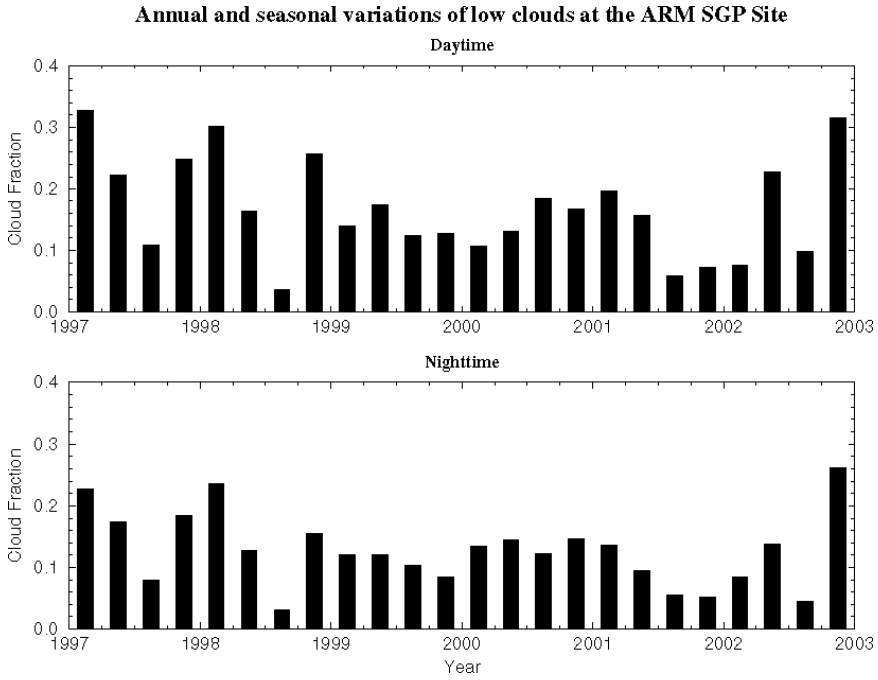

FIG. 1. Cloud fractions in each season at the ARM SCF, ~2163 h of samples (5-min resolution) used in this study for daytime, and ~1839 h for nighttime. The four seasons used in this study are DJF (winter), MAM (spring), JJA (summer), and SON (autumn) except the 1996/97 winter includes Jan and Feb 1997.

On the basis of sensitivity studies (D97) and comparisons with aircraft data (D98; Dong et al. 2002; Dong and Mace 2003a), the D98 parameterized cloud radiative properties should be accurate to about ±5%, while the r_e values have uncertainties of approximately 10% for daytime and 15% for nighttime. The uncertainties in the calculated cloud-droplet number density N can be up to 20%–30% for daytime and 30%–40% for nighttime because of uncertainties in the observed cloud boundaries and the assumption of a constant size distribution. The logarithmic width σ_x is set to 0.38 (Miles et al. 2000) in this study. Fixing σ_x in the cloud retrieval scheme does not lead to significant errors in the retrieved values of r_e, while N changes by 15%–30% as σ_x varies from 0.2 to 0.5 (D97).

3. Seasonal means and distributions of cloud properties

The four seasons are defined here as winter from December to February (DJF), spring from March to May (MAM), summer from June to August (JJA), and autumn from September to November (SON), except that the 1996/97 winter includes January and February 1997. The seasonal/annual averages, standard deviations, medians and modes listed in Table 2 are simply the statistics of all selected samples (5-min resolution) within a 3-month season using the previously noted criteria for all cloud properties during the 6-yr period. The seasonal cloud fraction standard deviations are calculated from six annual seasonal means.

a. Cloud fraction

The cloud fraction derived from the upward-looking narrow field-of-view radar/lidar pair measurements is simply the percentage of returns that are cloudy within a specified sampling time period—that is, the ratio of the number of hours when they satisfied the retrieval criteria to the total number of hours when all instruments (radar, lidar, microwave radiometer, and PSP) were working. Because of the overcast definition, which can also include fog and some large-celled stratocumulus clouds, frequency of occurrence and cloud fraction C due to these stratus clouds are synonymous in this study. This cloud fraction should not be confused with an instantaneous hemispheric cloud fraction observed by satellite observations and surface observers. Cloud fraction for the surface observer is the percentage of the sky dome covered by clouds, while for the satellite imager, it is the ratio of the number of pixels within some defined earth surface area. The Warren et al. (1986) time-averaged cloud fraction, compared with our study, is defined as the product of frequency-of-occurrence and amount-when-present.

The time series of seasonal mean daytime and nighttime cloud fractions are plotted in Fig. 1 and summarized in Table 2. The least amount of stratus occurred during the summer of 1998 while the greatest occurred

during winter of the previous year. On average, the seasonal variation of stratus is marked by minima during summer and maxima during winter (Table 2). But that cycle does not always hold. For example, the seasonal variation in single-layer stratus coverage was relatively small between 1999 and 2001 with the daytime maximum occurring during the summer in 2000 (Fig. 1). The interannual change in stratus coverage is very large. For example, during the six winters, the daytime cloud fraction ranged from 0.08 to 0.32, a factor of 4 in variation. Nevertheless, the coverage during winter is the least variable in a relative sense with standard deviations (SD) of 62% and 41% during daytime and nighttime, respectively (Table 2). The maximum interannual variability exceeds 100% during summer. On average, fewer single-layer stratus clouds occur at night than during the day, but the interannual variability is smaller at night, even in a relative sense.

b. Macrophysical properties

The seasonal mean values of Z_{base}, Z_{top}, ΔZ, T_{base}, and T_{top} from January 1997 to December 2002 at the ARM SCF are shown in Fig. 2 for both day and night. The heights are given in km above ground level. They can be converted to kilometers above mean sea level by adding 0.315 km, the surface elevation at the SCF. As shown in Fig. 2 and Table 2, the seasonal variations in the cloud macrophysical properties for both daytime and nighttime are almost the same. For the seasonal variation, the Z_{base}, Z_{top}, and ΔZ means are generally greater during summer than in winter, which suggests that warm layer clouds are higher and thicker than colder ones. The positive correlation between cloud height and temperature can be easily explained by the increased lifting condensation level (LCL) of surface air during summer (DW00) and by the much higher cloud temperatures in summer than in winter if their cloud heights are the same. For the vertical distribution within a specified time period, however, the cloud height normally has a negative correlation with cloud temperature; that is, the higher the cloud height, the lower the cloud temperature, as shown in the seasonal means of both summer and autumn. Even though the cloud heights are the same during the day and night within a season, the daytime cloud temperatures may be slightly higher than those at night (spring; Table 2). The cloud-base heights and temperatures tend to be higher and lower, respectively, at night than in the daytime during all seasons except winter when there is virtually no day–night difference. The average cloud-top altitude is around 20 m less at night compared to daytime during winter and spring, but is 80 m higher at night during summer and fall. The cloud-top and -base temperatures differ by only 0.3 and 1.5 K during winter and autumn, respectively, despite corresponding mean thicknesses of 0.66 and 0.74 km. The small temperature differences suggest a nearly isothermal atmosphere. During summer, the base-top temperature differences are greatest with an average of 3.75 K, which, when combined with the mean thickness (0.923 km) suggests a lapse rate of 4.1 K km^{-1}, a dramatically different structure compared to the winter and fall atmospheres that give rise to stratus clouds.

The probability distribution functions (pdf) and cumulative distribution functions (cdf) for these macrophysical properties are illustrated in Fig. 3 for day and night. During daytime (nighttime), the yearly median values of Z_{base} and Z_{top}, respectively, 0.74 (0.71 km) and 1.67 km (1.51 km), and the mode values of Z_{base} and Z_{top}, respectively, 0.5 (0.5 km) and 1.1 km (1.1 km), are generally less than their means (Table 2). Nearly 65% of the clouds have bases below 1 km and tops lower than 2 km during both day and night. Only 10% of the Z_{top} values are between 3 and 4 km confirming that the screening criteria are retaining nearly all relevant low clouds. Cloud-top heights are more broadly distributed than bases in all cases. The seasonal variation of ΔZ (Fig. 2c) is not as regular as the cycles in cloud heights and temperatures, despite the differences in its summer and winter means, which increase by ~0.3 km from winter to summer (Table 2). The most common cloud thickness, 0.3 km, is less than half of the mean thickness for all seasons except for summer. As a result of the day–night differences in Z_{top} frequencies, the frequency distribution of ΔZ is slightly broader during the daytime than at night. Nevertheless, 50% of the clouds are less than 0.7 km thick during day and 0.57 km thick during night indicating that the medians are close to the annual mean values.

The pdfs for T_{base} (Fig. 3d) and T_{top} (Fig. 3e) are slightly flatter during the day than at night with a distinct mode in both quantities around 273 K at night. Cloud-base temperature rarely (5%–10% of the time) exceeds 295 K or falls below 260 K. Despite the mode at 273 K, supercooled liquid water (SLW) or ice occurs in only 30% of these clouds during both day and night. The temperatures in most of the clouds are between 265 and 290K, and the order of mean, median, and mode values for all four seasons and year is nearly opposite to that of cloud heights, that is, from minimum to maximum. From Fig. 3 and seasonal pdfs and cdfs of cloud heights and temperatures (not shown), it is concluded that the percentages of SLW for winter, spring, summer, and fall seasons are approximately 60%, 27%, 3%, and 19%, respectively. Since the ARM SGP does not have depolarization lidar, it is not possible to identify separately the liquid and ice phases, or mixed phase in these clouds ($T < 273$ K).

c. Microphysical properties

Figure 4 shows the daytime and nighttime seasonal means, respectively, of cloud microphysical properties, LWP, LWC, r_e, and N. Their corresponding frequency distributions are plotted in Fig. 5 and their seasonal and yearly mean, standard deviation, median, and mode values are listed in Table 2. The seasonal variations in

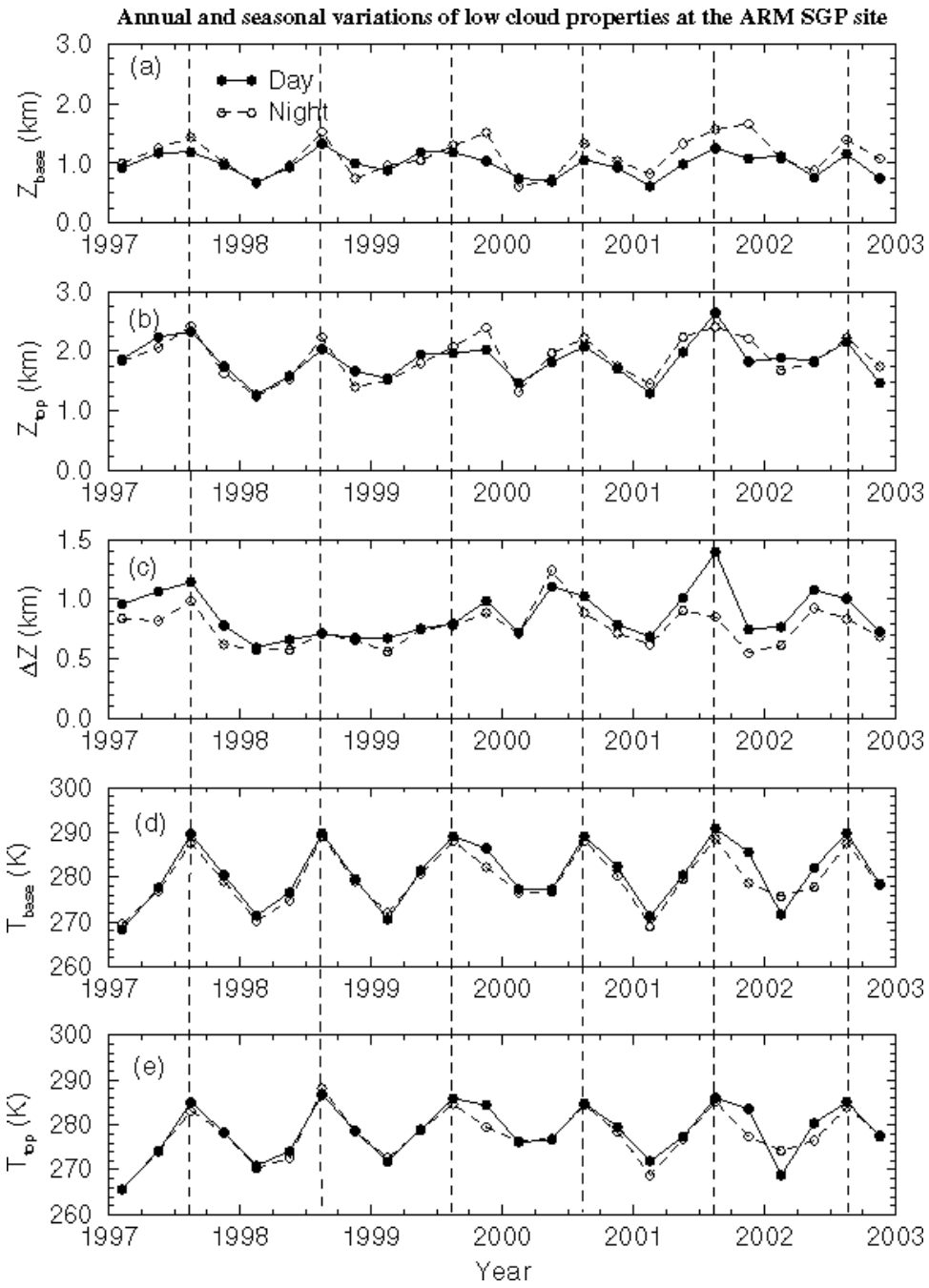

FIG. 2. Seasonal means of daytime (●) and nighttime (○) low cloud macrophysical properties at the ARM SCF from Jan 1997 to Dec 2002. The dotted lines represent six summers during the 6-yr period.

LWP for both daytime and nighttime are obvious (Fig. 4a); they reach a minimum in summer and have maxima in spring and fall. Nearly all mode values are half of their mean values, and their medians are in the middle between mode and mean. The yearly mean, median, and mode values are about 145, 106, 75 g m^{-2}, respectively. Cloud LWC, the ratio of LWP to ΔZ, decreases during each summer relative to the preceding seasons (Fig. 4b). The LWC modes and medians (Table 2) are 0.075 and 0.20 g m^{-3} for daytime and 0.1 and 0.232 g m^{-3} for nighttime, respectively. The median LWC values are close to their means but their modes are much smaller than their means. The daytime and nighttime seasonal variations in cloud-droplet number concentration (N) are very similar to those for LWP and LWC, that is, minima in summer and maxima in winter

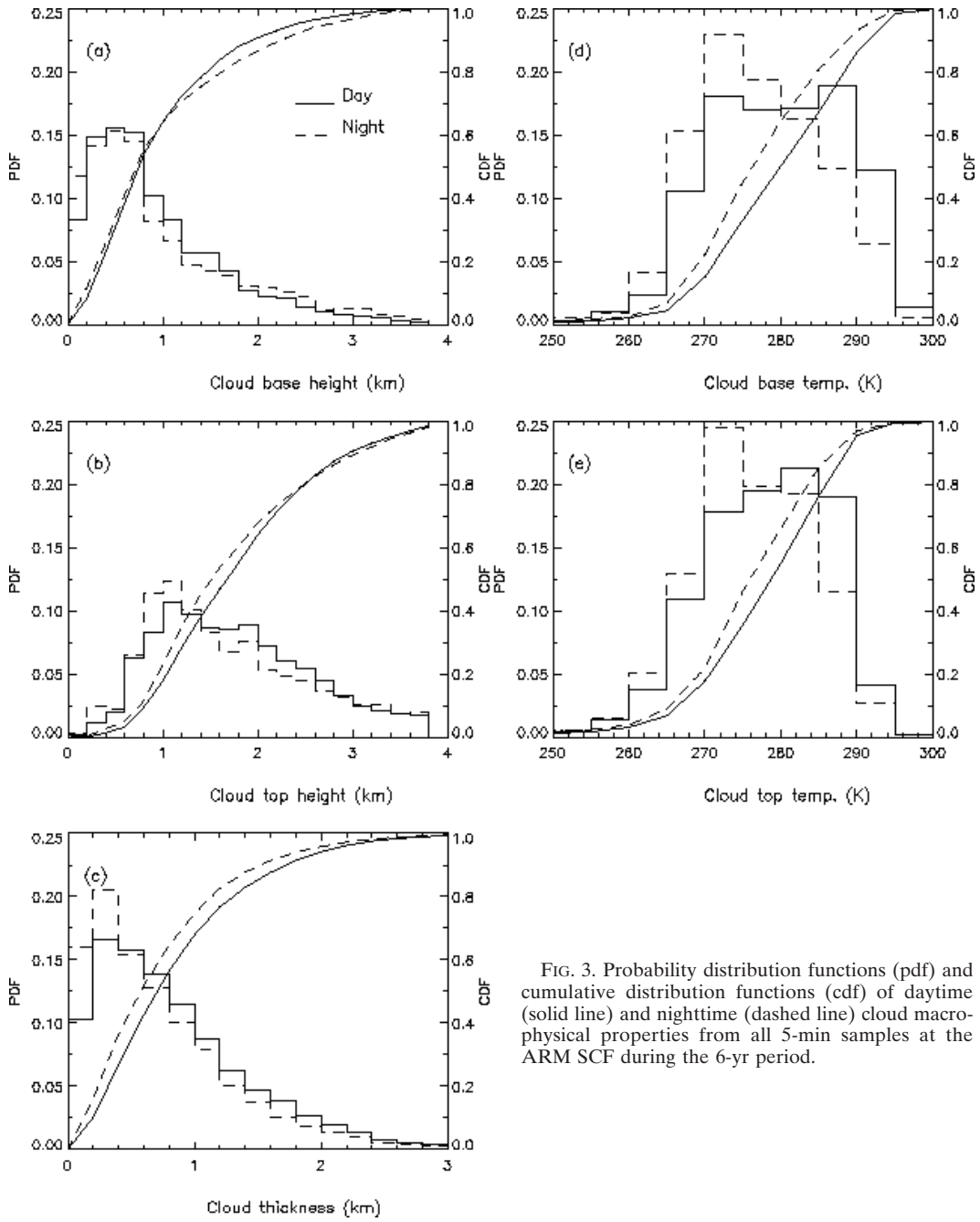

FIG. 3. Probability distribution functions (pdf) and cumulative distribution functions (cdf) of daytime (solid line) and nighttime (dashed line) cloud macrophysical properties from all 5-min samples at the ARM SCF during the 6-yr period.

(Fig. 4d). The mean value of N during winter, ~273 cm^{-3}, is double that during summer, 143 cm^{-3}. The yearly modes and medians for N (Table 2) are 25 and 117 cm^{-3} for daytime and 25 and 150 cm^{-3} for nighttime, respectively. The seasonal and yearly median values are nearly half, and mode values are about 10%–20% of their mean values. The seasonal and yearly means of cloud-droplet effect radius (r_e) for both daytime and nighttime are almost identical as shown in Table 2. Their median values range from 7.8 to 8.4 μm, and mode values from 7.0 to 8.0 μm. The seasonal variations in r_e (Fig. 4c) are not as strong as those in LWP, LWC, and N. The yearly modes and medians of r_e (Fig. 5c) are nearly the same for both day and night with average values of 7.5 and 8.1 μm, respectively. In the frequency distributions, N has a long tail toward higher values, while r_e is more normally distributed.

d. Radiative properties

The time series of the seasonal mean daytime and nighttime broadband cloud optical depths, effective solar transmission, R_{cldy}, and R_{TOA} are plotted in

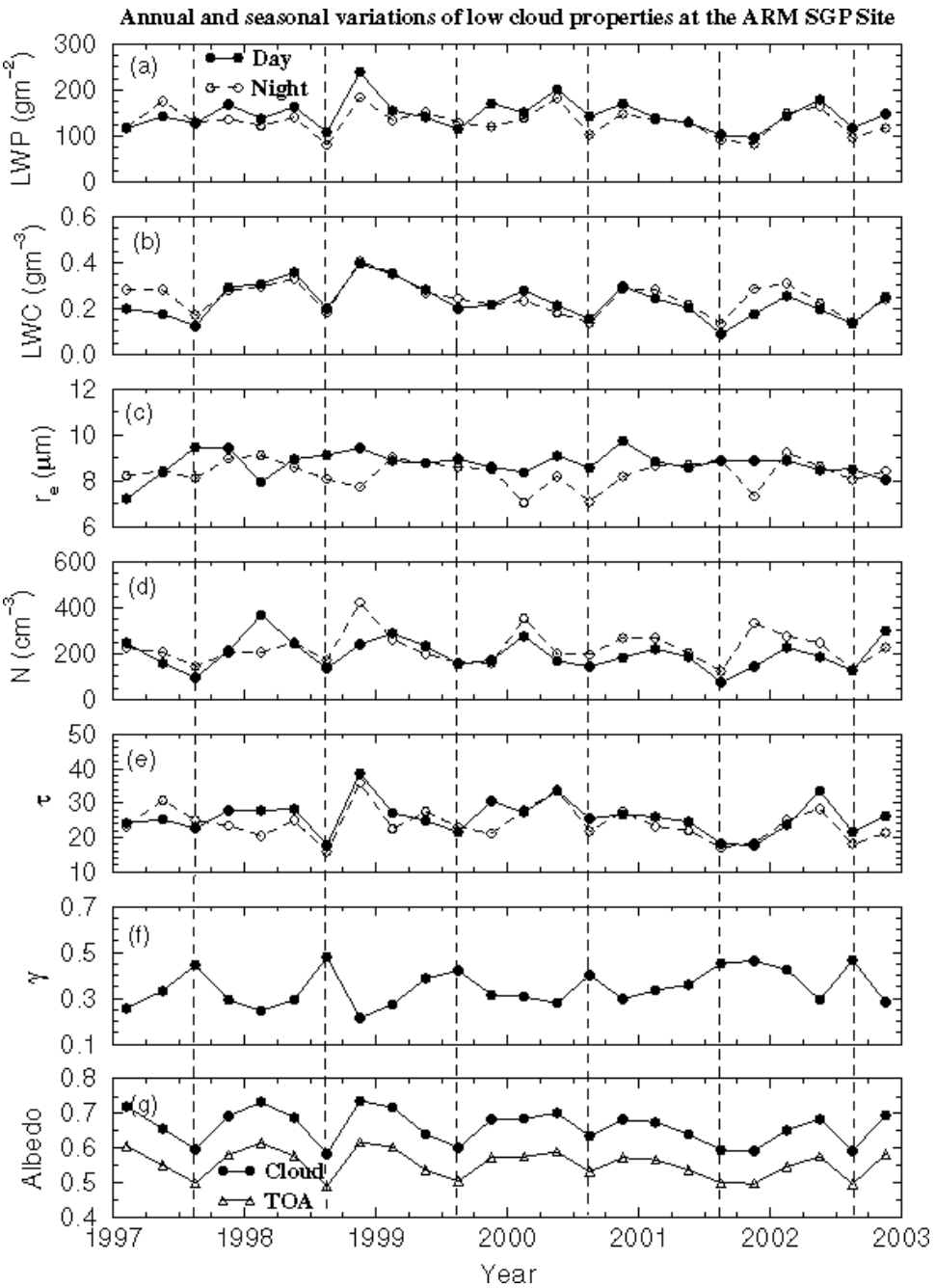

FIG. 4. Seasonal means of daytime (●) and nighttime (○) low cloud microphysical and radiative properties at the ARM SCF from Jan 1997 to Dec 2002. The dotted lines represent six summers during the 6-yr period.

Figs. 4e–g. Their corresponding frequency distributions are shown in Figs. 5e–h. Since there are no strong seasonal variations in r_e, the variations in the seasonal means of τ for both daytime and nighttime basically follow the variation in LWP. Most τ values (>90%) are between 5 and 60 with peaks and medians at 7.5 and 21.2 for daytime, and 12.5 and 20 for nighttime. The lower limit of τ (=5) is artifact of the lower limit (=20 g m^{-2}) of LWP used in this study (criterion 3). The yearly means and standard deviations of τ are, respectively, 26.8 and 19.9 for daytime, and 24.8 and 18.9 at night (Table 2). The negative correlation between τ and the measured values of γ, while expected, is based on the model estimate of τ using γ and LWP as constraints. The peak frequency of occurrence of γ is 0.175 with the median and mean values of 0.28 and 0.331. Like most of

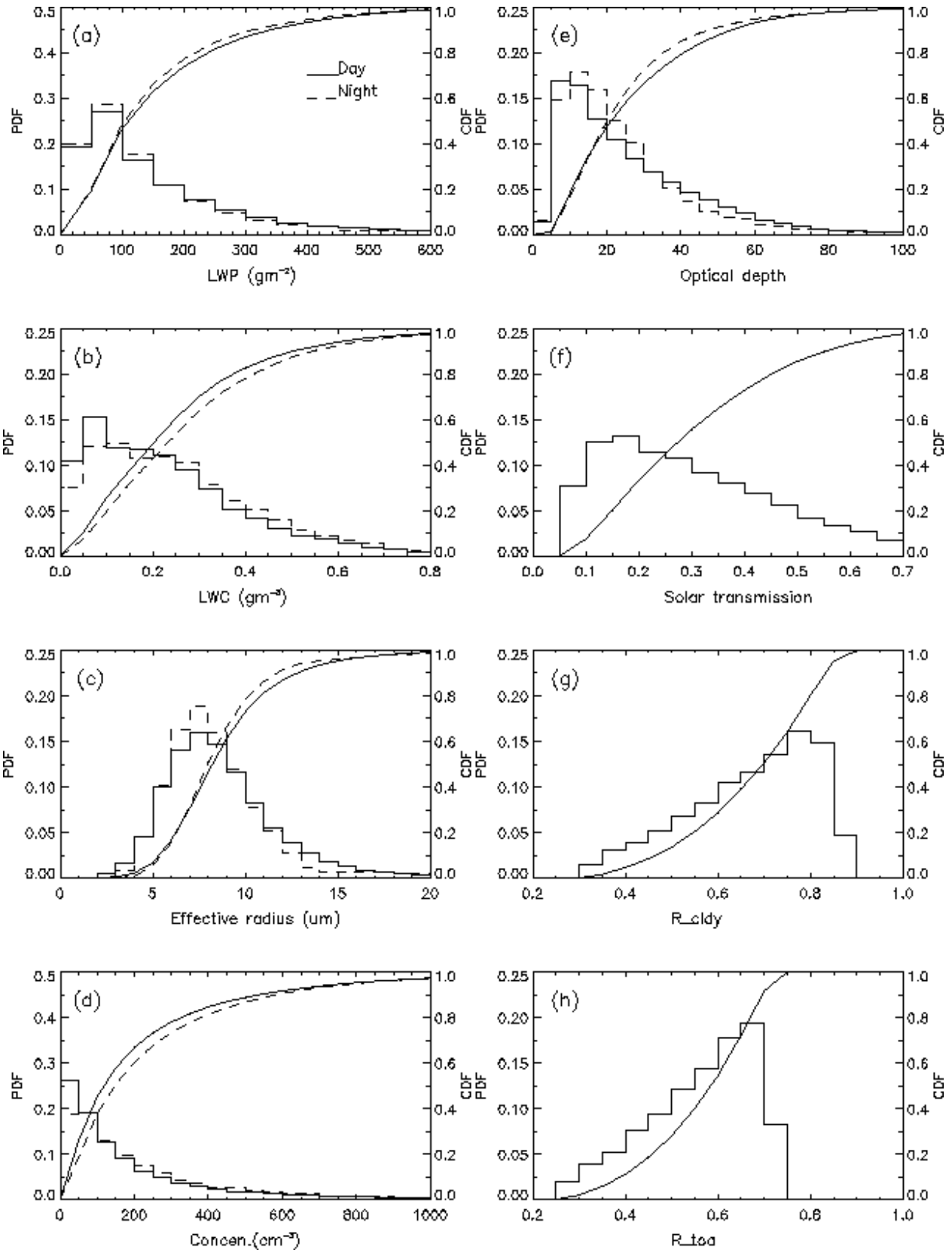

FIG. 5. Pdf and cdf of daytime (solid line) and nighttime (dashed line) cloud microphysical and radiative properties from all 5-min samples at the ARM SCF during the 6-yr period.

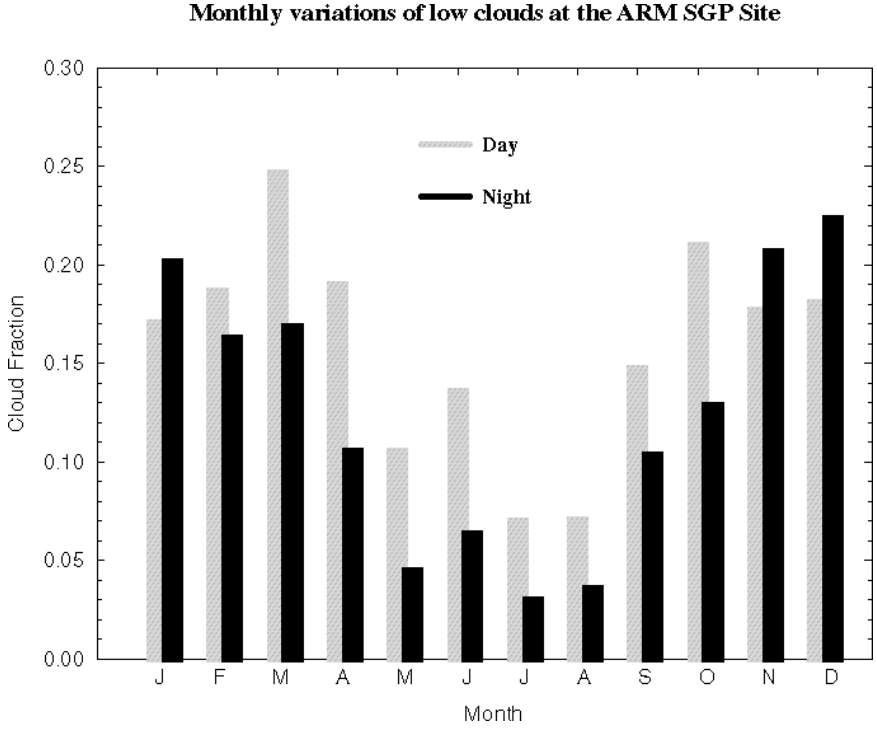

FIG. 6. Same as Fig. 1, except for monthly cloud fraction derived from the 6-yr ARM SCF dataset.

the previously discussed variables, the pdf tails off gradually at higher values. Because R_{cldy} and R_{TOA} are positively correlated with τ, they increase with rising τ. The frequency distributions of R_{cldy} and R_{TOA} are also broad but have longer tails toward smaller values. The mode, median, and mean values of R_{cldy} are 0.775, 0.697, and 0.672, respectively. The corresponding values for R_{TOA} are 0.675, 0.584, and 0.563.

4. Monthly means and variabilities of cloud properties

To further refine the temporal variability, the monthly means and variations were calculated using all samples (both day and night) for a given month during the 6-yr period. The monthly cloud fraction during the 6-yr period is illustrated in Fig. 6. Naturally, the variability in monthly mean cloud fraction is similar to its seasonal counterpart seen in Fig. 1. The minimum cloud fractions occur during July and August, while the maxima occur in March and October for daytime and in January, November, and December for nighttime. The greatest low stratus cloud occurrence is during March while the least is in July for both daytime and nighttime.

Monthly means and distributions of combined daytime and nighttime macrophysical and microphysical cloud properties derived from the 6-yr ARM SCF dataset, represented as box-and-whiskers plots, are shown in Figs. 7 and 8, respectively. In each plot, the bottom and top of the box represent the 25th and 75th percentiles of the distribution, the bottom and top of the whisker represent the 5th and 95th percentiles of the distribution, and the shorter and longer lines across each box represent the median and mean, respectively. The distribution at the far right (ANN) of each plot shows the cumulative statistics from the entire dataset (both day and night) during the 6-yr period and the average from the entire dataset is given by the horizontal line extending across the entire plot. The mean Z_{base}, Z_{top}, T_{base}, and T_{top} values (Figs. 7a–b,d–e) show a strong peak from May to September and the ΔZ mean values (Fig. 7c) are above the yearly average from April to September. The cloud-base parameter means vary smoothly with month. Monthly mean values of LWP, LWC, N, and τ (Figs. 8a–b,d–e) all show dips from May to August with local maxima occurring around February–March and November–December. Again, there is no apparent monthly pattern in the mean r_e (Fig. 8c). The monthly means of γ and R_{cldy} (Figs. 8f–g) are as expected from the seasonal data, the maximum in γ and the minimum in R_{cldy} occur during July–August, then vice versa during January–February.

5. Diurnal variability

The cloud properties were averaged by local hour to detect any diurnal cycles in each parameter. The hourly means and variations were calculated from all samples

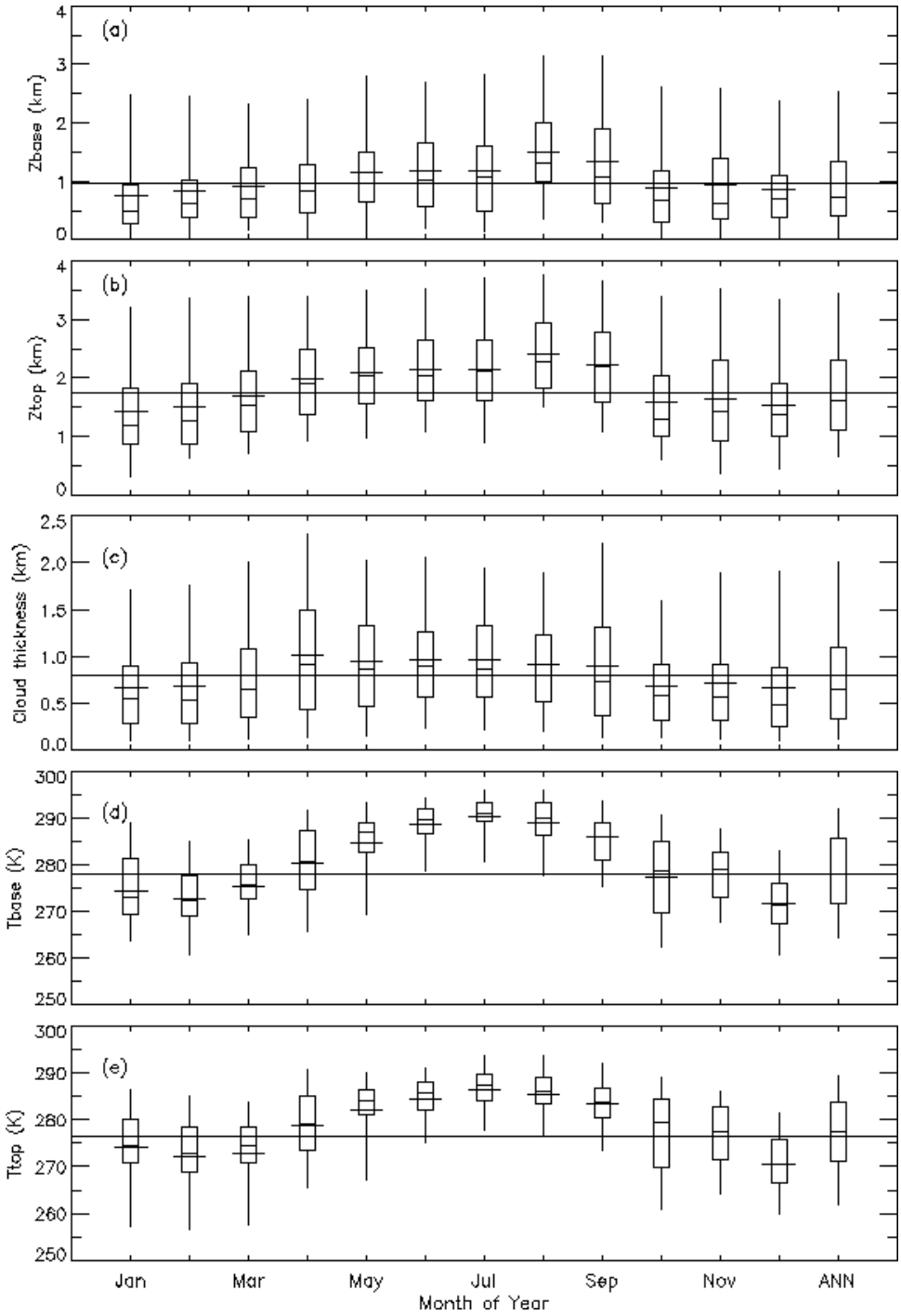

FIG. 7. Monthly averages of combined daytime and nighttime cloud macrophysical properties from the 6-yr ARM SCF dataset. The bottom and top of the box represent the 25th and 75th percentiles, the bottom and top of the whisker represent the 5th and 95th percentiles, and the shorter and longer lines across each box represent the median and mean, respectively. The distribution at the far right (ANN) of each plot shows cumulative statistic from both daytime and nighttime datasets during the 6-yr period, and the yearly average from entire dataset is drawn across the entire plot.

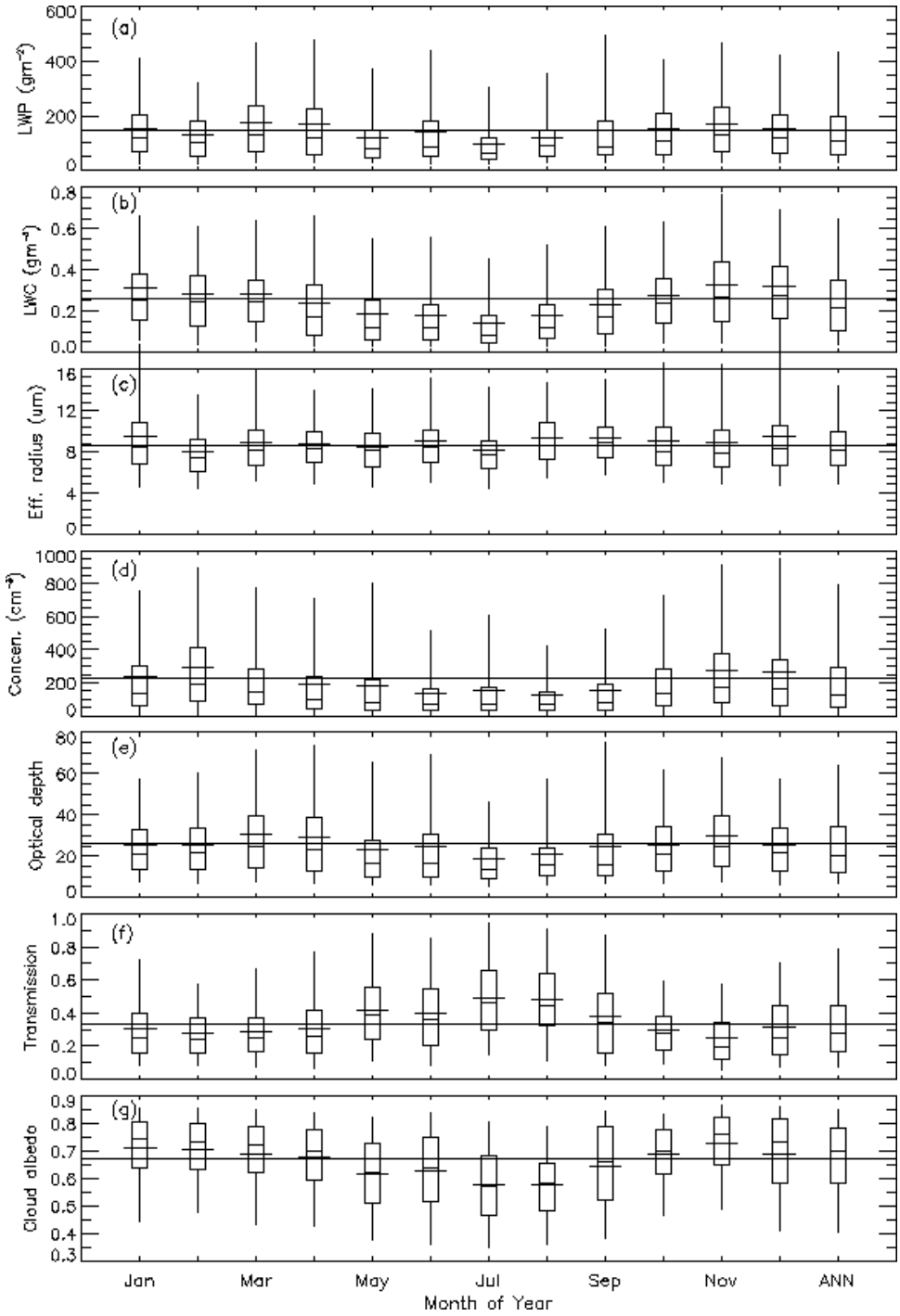

FIG. 8. Same as Fig. 7, except for cloud microphysical properties. The radiative properties, transmission, and cloud albedo are derived from the daytime dataset only.

in that hour from the 6-yr ARM SGP dataset. The mean hourly cloud fractions are plotted in Fig. 9 for all of the data and for summer and winter separately. In the annual average (Fig. 9a), cloud amount increases almost monotonically from midnight [(0000 local time (LT)] to 0930 LT. The broad maximum during midday is followed by a decline in C until 1930 LT when it levels off for the remainder of the night. This same diurnal cycle is seen during both extreme seasons. Although the summer (~0.09; Fig. 9b) and winter (~0.07; Fig. 9c) cloud fraction variations are nearly the same, the difference in relative variation is large. For ex-

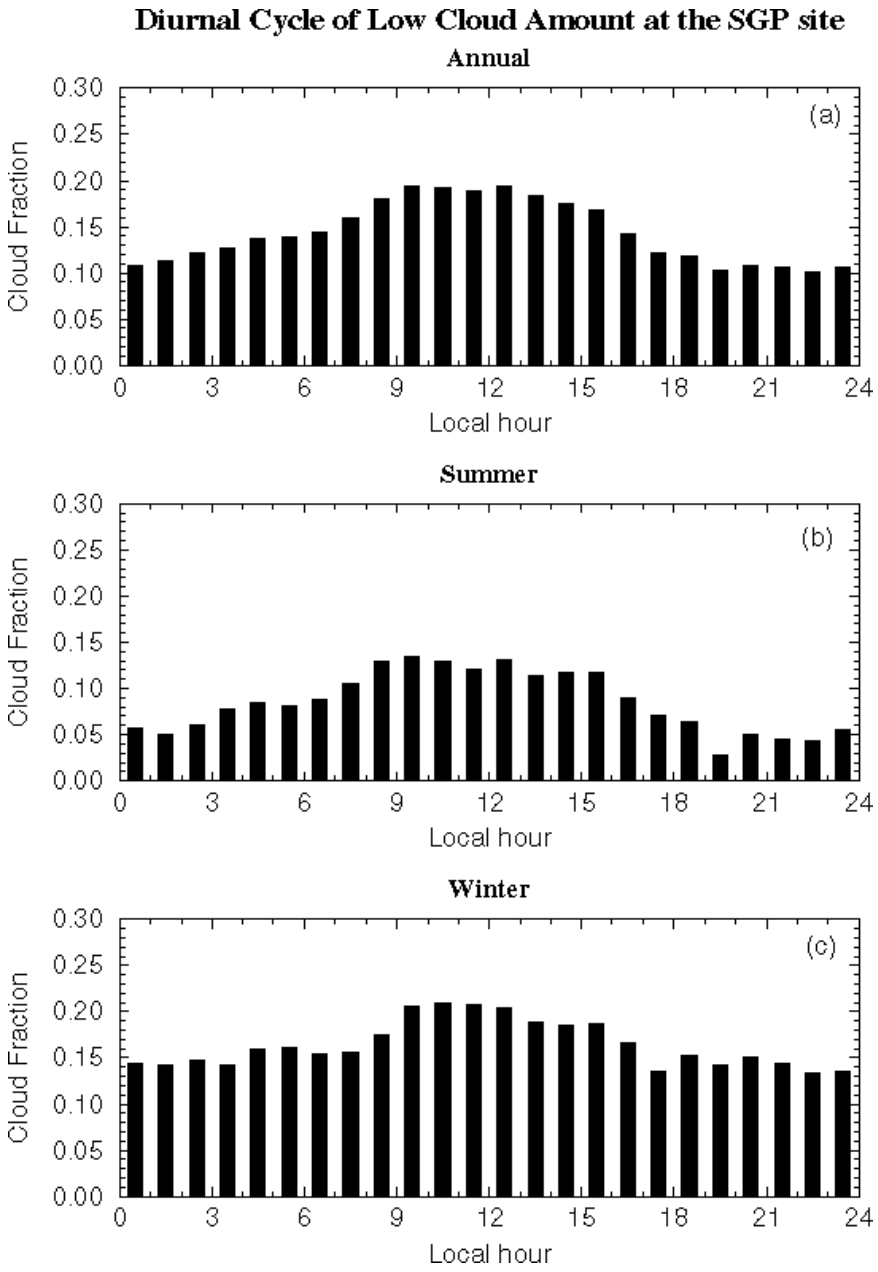

FIG. 9. Same as Fig. 1, except for hourly cloud fraction derived from both daytime and nighttime datasets at the ARM SCF during the 6-yr period. The ARM SCF local noon is ~1230 LT (UTC = local time + 6 h).

ample, the summer cloud fraction increases from 0.05 to 0.14 (180%) and the winter cloud fraction rises from 0.14 to 0.21 (50%) from the midnight to local noon. This suggests that the diurnal cycle during the summer is much stronger than during the winter due to the summertime local convection at the SCF.

The corresponding hourly means and variabilities for each cloud property are illustrated in Fig. 10, where the definitions of the lines and symbols are the same as those for the results in Fig. 7. The Z_{base} and Z_{top} averages are generally lower than the daily mean by about 0.1–0.2 km in the morning, and higher by about the same amount in the afternoon (Figs. 10a,b). The hourly mean values of T_{base} and T_{top} (Figs. 10d–e) vary in patterns opposite to those for the height parameters because cloud temperature normally decreases with increased cloud height. Mean cloud thickness (Fig. 10c) increases by approximately 0.2–0.3 km from a minimum around 0430 LT to a maximum around 1130 LT. It is relatively invariant between 0900 and 1400 LT. The

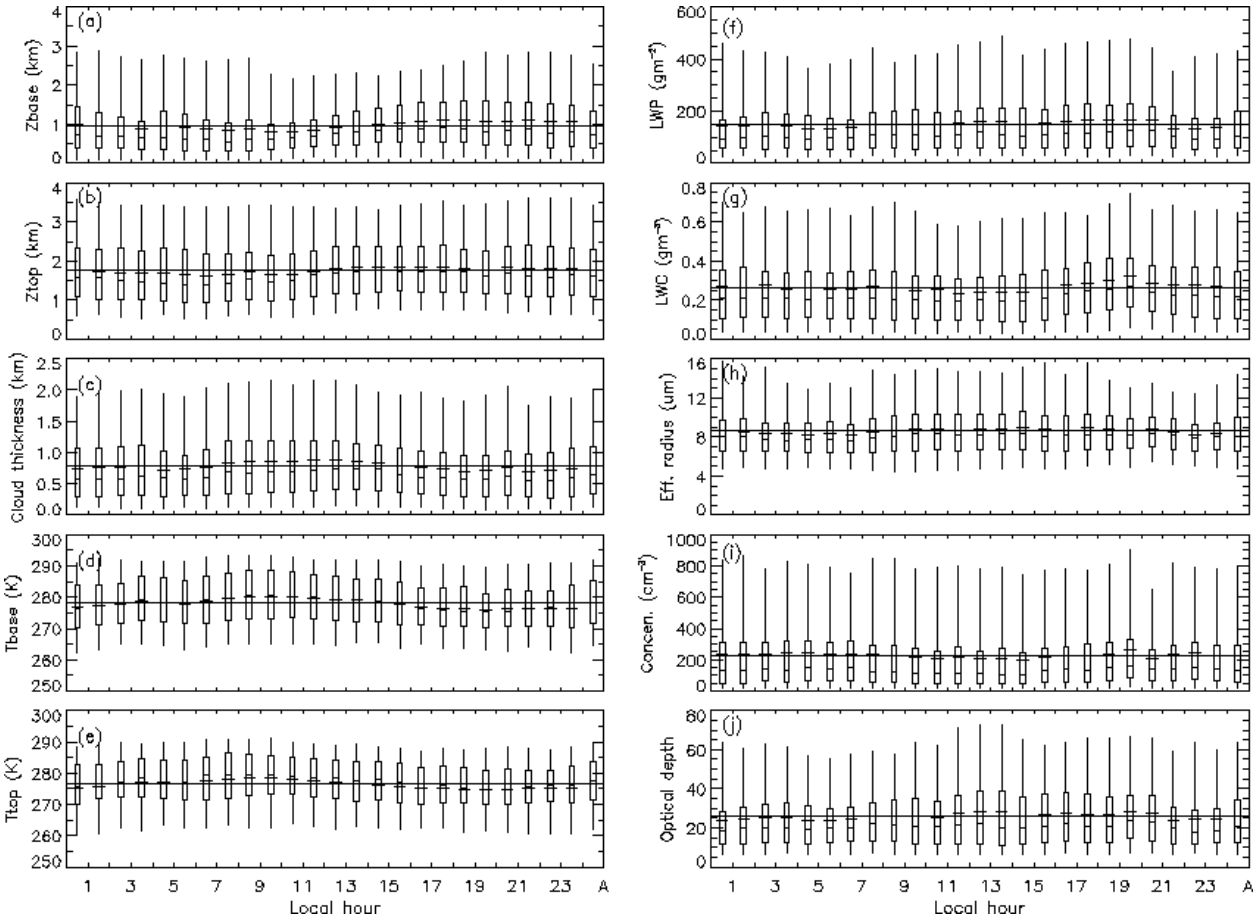

FIG. 10. Same as Fig. 7, except for hourly means of low cloud properties from both daytime and nighttime datasets. The distribution at the far right (A) of each plot shows cumulative statistic from both daytime and nighttime datasets during the 6-yr period, and the yearly average from entire dataset is drawn across the entire plot.

magnitude of the ΔZ hourly anomalies are similar to those of Z_{base} and Z_{top}, but in the opposite direction. This result indicates that the low stratus clouds at the ARM SCF site are lower, warmer, and thicker in the morning compared to those observed during the afternoon. LWC increases from morning to afternoon as shown in Fig. 10g, which suggests that the low, warm, and thick clouds have less LWC, while the high, cold, and thin clouds have more LWC. LWP and N have a similar pattern to LWC, but much weaker. Since there is no strong diurnal cycle in r_e, the diurnal variation of τ basically follows that of LWP.

6. Discussion

a. Cloud fraction

The cloud fractions in Table 2 are restricted to the conditions of single-layer and overcast low clouds. However, analysis of all low cloud cases (not shown), including those with overlying mid or high-level clouds, yields cloud amount patterns that are very similar to those in Fig. 1. The results are consistent with the data of Warren et al. (1986) for an 11-yr average of surface observations in a 5° region centered near the SCF. The four seasonal means of SSF (stratus + stratocumulus + fog) cloud amount from Warren et al. (1986) are 0.25, 0.23, 0.07, and 0.22, a pattern that is similar to that in Table 2. The greater amount of SSF cloud cover is probably due to the requirement of overcast (cloud base/top seen continuously by the lidar/ceilometer/radar for ~2 h) and single-layer clouds in the current dataset. The surface data include nonovercast low clouds and low clouds with other clouds above them, and, therefore, should yield greater cloud amounts than seen in Table 2. The amount of overlapped stratus is difficult to determine from the surface, however, because the upper levels of the troposphere cannot be observed when obscured by a low overcast. This difficulty is highlighted in the multilayer statistics of Warren et al. (1984). For the 5° region encompassing the SCF, the surface climatology indicates that SSF clouds are observed only about 30% of time without another layer present, yet the presence or absence of middle and

high-level clouds can only be determined about 75% of the time. Thus, the 30% value probably corresponds only to stratocumulus clouds and may not represent the single-layer stratus probability.

Compared to the SSF surface climatology (Warren et al. 1986), the diurnal variations in single-layer low cloud amount (Fig. 9) differ in phase but have similar amplitudes. The surface data indicate that SSF coverage peaks at 0800 LT while cumulus coverage maximizes around local noon. In Fig. 9, the maximum actually extends over a 4–5-h period between 0900 and 1300 and could just as easily be assigned to 0900 LT as any other hour. The climatology is based on 3-hourly data so that a 0900-LT peak would not be statistically different than one at 0800 LT. Additionally, some slight difference is expected between the two datasets because of differences in the sampled populations discussed earlier and in the definitions of low clouds.

Minnis and Harrison (1984) also found a morning maximum in low clouds over the central United States from hourly geostationary satellite data, but only reported results for 1 month. Del Genio et al. (1996) compared GCM simulations with the International Satellite Cloud Climatology Project (ISCCP) climatology and found that, over midlatitude land areas, the diurnal cycle of low clouds peaked in the morning and early afternoon in the GCM and ISCCP results, respectively. Both model and observational data agree, at least, that the maximum occurs during the time interval defined by the broad maximum in Fig. 9 and not during the night or early morning. This differs from the broad maximum in marine stratus and stratocumulus coverage, which tends to have a broad peak centered on ~0600 LT suggesting different formation and dissipation mechanisms.

b. Cloud macrophysical properties

The relative seasonal variation in Z_{base} is the same as that in the surface climatology (Warren et al. 1986)—that is, the lowest in winter and the highest in summer, but the surface-observed Z_{base} values, ranging from 0.64 to 0.90 km from winter to summer, are roughly 0.2 km lower than those in Table 2. Although Z_{base} in Warren et al. (1986) was sometimes measured, it was mostly estimated subjectively. The seasonal variations of Z_{base} from the ceilometer also agree well in a relative sense with those of the DW00, although the current values are roughly 0.2 km higher than those from DW00 during winter and almost 0.4 km higher during summer. Differences in cloud-base height may be due to the inclusion of nonovercast low cloud cases by DW00 and Warren et al. (1986) or to a different interpretation of the ceilometer data. The Z_{top} values in DW00 are ~0.9 km greater than those in Table 2 for the winter season, but are in excellent agreement during summer. The results are large differences in ΔZ. The averaged ΔZ values in the DW00 are 1.42 and 1.80 km for warm and cold seasons, respectively, compared to 0.92 and 0.65 km from the current Table 2. These differences, which could be due primarily to either differences in methodology or the sampled populations, are important to understand because they affect the retrieval of LWC and N.

The clouds sampled by DW00 were single-layered low liquid-water clouds that were not necessarily overcast in the 2-h sense used here. Their only requirements for low cloud cover were that the cloud was observed by the ceilometer for 5 min with a base below 3 km; the mean infrared (IR; 10.8 μm) brightness temperature T_{IR} of the nearest four 4-km pixels from the Geostationary Operational Environmental Satellite (GOES) was greater than the temperature at 680 hPa as determined from the nearest sounding; and the range in T_{IR} for those four pixels was less than 5 K. The cloud-top temperature was given the value of T_{IR} and the cloud-top altitude corresponds to the altitude Z with temperature $T(Z)$ in the sounding that is equal to T_{IR}. It was found by comparing T_{IR} with $T(Z)$ starting at 680 hPa (~3 km) and proceeding downward through the sounding until $T(Z) > T_{\text{IR}}$. This approach does not account for attenuation of the IR radiance by the atmosphere, an effect that will cause some overestimate of the cloud-top height. The cloud-base height was taken as the average altitude from the ceilometer returns and the cloud-base temperature was obtained directly from the sounding. Thus, the DW00 clouds could include stratus, stratocumulus, fog, cumulus, and any multilayered clouds with tops below 680 hPa. During winter, cumulus is rarely observed over the Great Plains (Warren et al. 1986). Thus, more cold season fog, stratocumulus, and multilayered low clouds were probably observed by DW00 because they would be the only low clouds that would be observed besides those defined for this study (cumulonimbus and nimbostratus would be too thick to qualify). Neither cloud type tends to have much vertical development. Cumulus clouds, which have greater vertical development than stratus, climatologically account for a cloud amount of 0.05 during summer, slightly less than the overcast amount observed in this study (Table 2). Therefore, the DW00 sample probably included a significant portion of cumulus clouds in addition to the relatively flat overcast clouds that comprise the results in Table 2. The sampling difference could explain, at least, some part of the Z_{top} and ΔZ discrepancies for both summer and winter.

Determination of a cloud height from T_{IR} and a sounding is not as straightforward as it might seem if inversions are present (e.g., Garreaud et al. 2001). From this study, we found that there are more above-cloud inversions during winter than in summer when convection is common. These strong above-cloud inversions during winter might be one of the reasons for leading to the discrepancy between DW00 and this study. Therefore, we summarize the following possible

reasons to explain the differences in Z_{top} during the winter between this study and DW00: 1) cloud sampling difference, such as overcast versus all low clouds, single layer versus multilayer; 2) T_{IR} error due to above-cloud temperature inversions; 3) T_{IR} error due to the lack of atmospheric water vapor correction; 4) the uncertainties of Z_{top} derived from MMCR reflectivity; and 5) optically thin cirrus clouds above low clouds, those were not screened out by MMCR or beyond the limitation of MMCR detection to thin cirrus clouds ($\tau \sim 0.1$, Wang and Sassen 2002). The 20% of these optically thin cirrus clouds ($\tau < 0.1$), detected by the Raman lidar but were not detected by MMCR (Wang and Sassen 2002), do not affect the MMCR-derived Z_{top} and only slightly increase T_{top}. However, those cirrus clouds can easily make satellite T_{IR} colder than its actual T_{top}, and overestimate its Z_{top}.

Another issue that should be mentioned is that the MMCR-derived Z_{top} values during summer in this study may be biased high, at times, due to insect contamination of the MMCR reflectivities. The magnitude of the bias will depend upon the month and time of day, and this problem will not be solved until an operational 94-GHz cloud radar is installed at the ARM SGP site (E. E. Clothiaux and G. G. Mace 2004, personal communication). Therefore, Z_{top} values from late spring to early fall should be used with caution. Note that Dong et al. (2000) used radiosonde soundings to estimate ΔZ and Z_{top}. They did this by taking cloud to occur in the vertical extent of the lower atmosphere where the relative humidity exceeded 94% during the periods when clouds were known to exist from MMCR and lidar/ceilometer measurements. They subsequently used the radiosonde-derived ΔZ to modify the MMCR-derived Z_{top} values during the summers of 1997 and 1998. They made the modification by setting Z_{top} equal to the sum of the radiosonde-derived ΔZ and the lidar/ceilometer-detected Z_{base} for those times when the MMCR-derived Z_{top} values were higher than the cloud tops in the radiosonde soundings. Comparing the current Z_{base} and Z_{top} with the Dong et al. (2000) results for the period January 1997—November 1998, we found that both the current Z_{base} and Z_{top} values are consistently higher by approximately 400–500 m than the Dong et al. (2000) results. However cloud thicknesses in the two studies were almost identical. The Dong et al. (2000) results were derived from preARSCL retrievals, which were biased low by approximately 200 m because of processing errors (E. E. Clothiaux 2000 and 2004, personal communication). Adding 200 m to the Dong et al. (2000) values, the current Z_{base} and Z_{top} values are still ~200–300 m higher than the Dong et al. 2000 results. If the current Z_{top} values are biases high by 200–300 m because of insect contamination, we would expect the current cloud thicknesses to exceed those of Dong et al. (2000), which they do not. While this result does not conclusively prove that the current Z_{top} values are not biased high, this result does indicate that the bias may not be significant.

c. Cloud microphysical properties

The ΔZ difference between DW00 and this study could also help explain why the cloud LWC values from DW00 and Table 2 are similar during the summer, but not in the winter. During the cold season, the current mean LWC is almost 3 times greater than that from DW00, nearly the same ratio of the DW00 thickness to ΔZ reported in Table 2. The mean LWP here is roughly 20% less than that from DW00 during winter and is 37% less during summer. The differences are probably due to (i) the lower and upper limits (20–700 g m^{-2}) in this study and 40–1000 g m^{-2} in the DW00 study; (ii) sampling of different clouds, especially in summer; and (iii) differences in the years and changes in the processing algorithm used by ARM to derive LWP (Liljegren et al. 2001) since the DW00 study. Nevertheless, the change of mean LWP with mean cloud temperature is similar to that found by DW00 for instantaneous values. These results indicate that, for the range of temperatures seen here, LWC increases with decreasing mean cloud temperature, and its correlations are -0.577 and -0.646 for day and night, respectively. LWP also has a slightly negative correlation with cloud mean temperature with values of -0.21 and -0.31 for day and night, respectively. These findings are based on 24 seasonal means in this study and therefore should be viewed with caution. The seasonal variations in LWC are also due to 1) small LWP and large ΔZ in summer and 2) large LWP and small ΔZ in winter, which suggests that the colder and thinner clouds have more LWC and LWP than warmer and thicker clouds. The results in Table 2 and Fig. 8b show that mean LWC decreases with increasing temperature, a dependence that is probably due to greater entrainment of dry air in the more convective conditions occurring during summer while during winter the strong inversions can capture most of water vapor to form clouds. A complete understanding of the quantitative correlations between cloud LWP/LWC and temperature and detailed physical explanation for these phenomena can only result from higher temporal resolution data (such as 5 min) and a combined effort with cloud-resolving or single column models; but they are beyond the domain of this paper.

The mean effective droplet sizes are relatively invariant with season while the number concentration during winter is twice its summer value for both day and night as shown in Figs. 4 and 8, and Table 2 with mode values of 50 and 25 for winter and summer, respectively. These lower mode values are plausible for maritime stratus clouds but not over the midlatitude continental ARM SGP site. Since N is calculated from the r_e and LWC values using a fixed lognormal size distribution, it is necessary to discuss the accuracies of r_e and LWC, as

well as the seasonal variations of aerosol concentrations. The values of N derived here are within the range reported by Miles et al. (2000). The winter means in this study are nearly the same as the average (288 cm^{-3}) from the Miles et al. (2000) data. For statistical comparisons of the r_e values with others, the means in Table 2 are nearly identical to the value obtained by Han et al. (1998) for Northern Hemisphere continental clouds using satellite data. Sengupta et al. (2003) found that a peak value of $r_e = 7.5$ μm, which is the mode value for the current dataset as listed in Table 2, yields the best fit between the observed and calculated solar transmission using the observed LWP*s* at the SCF. The annual mean value of r_e, however, is about 3-μm larger than the average r_e (5.4 μm) found by Miles et al. (2000) from a compilation of aircraft in situ data taken in clouds formed in continental air. The compilation includes data taken from a variety of instruments, sites, and locations within the cloud making it difficult to conclude if the present results should be the same as that aircraft summary. Given the excellent agreement with aircraft data reported by Dong et al. (1998, 2002; Dong and Mace 2003a) for a subset of the current dataset and the consistency with the Han et al. (1998) and Sengupta et al. (2003) results, it is concluded that these results are a good representation of the droplet sizes in low-level clouds over the SCF.

Note that the influence of surface albedo (R_{sfc}) on the r_e values was not directly included in the cloud-droplet effective radius parameterization of D98, but implicitly included in the solar transmission ratio, γ. The D98 parameterization was developed from two datasets: ASTEX ($R_{sfc} = 0.06$) and ARM SGP ($R_{sfc} = 0.18$). A sensitivity study revealed that the r_e difference could be 0.66 μm using the D98 parameterization and other radiative transfer model for the two surface albedos with fixed LWP (150 g m^{-2}) and solar zenith angle (45°). The monthly R_{sfc} means of cloudy conditions during the 6-yr period (Dong et al. 2004, manuscript submitted to *J. Climate*) range from 0.192 to 0.222, except for snowing periods during December (0.266), with an annual average of 0.211. The daily variation of R_{sfc} may be slightly larger than the monthly mean, but a lower limit of $\mu_0 = 0.2$ was applied in the D98 parameterization. Therefore, the R_{sfc} difference should never exceed 0.1 in calculating r_e values using the D98 parameterization. To further test the accuracy of the D98 parameterization, the Dong et al. (1997) retrieval was applied to 3 months (December 1997–February 1998) of data from the ARM SCF compared to the estimated r_e values from the D98 parameterization. Three monthly means from the retrievals and parameterization are 7.40 and 7.24 μm for December 1997, 9.4 and 9.72 μm for January 1998, and 7.43 and 7.41 μm for February 1998, respectively. Comparing with aircraft in situ measurements, the averaged r_e values of the aircraft and the D98 parameterization are 6.7 and 7.7 μm, a total of 5 h of data during the October 1996 Penn State IOP; and 7.9 and 7.6 μm, a total of 10 h of data during the March 2000 ARM SGP IOP, respectively. Given the small R_{sfc} variation at the ARM SGP, excellent agreement between the parameterization and retrievals, as well as aircraft in situ measurements, we can conclude that the D98 r_e parameterization is not significantly affected by R_{sfc} when R_{sfc} is small. However, it is affected when R_{sfc} is high, when the surface is snow covered. A further study supports the above conclusion (Dong 2005, manuscript submitted to *Geophys. Res. Lett.*).

Since the r_e values are relatively invariant with season, the seasonal variation of N mimics the LWC pattern where the mean and median values of LWC during the winter are almost twice their summer values, which is the major source for explaining the winter–summer difference in N. The low mode of N in Fig. 5 is mainly contributed by the low mode of LWC, especially during the summer seasons. The probabilities of N are ~0.4 at the mode value of 25 cm^{-3} during the summer and ~0.17 at the mode value of 50 cm^{-3} in the winter. The corresponding LWC mode values are ~0.3 and 0.075 g m^{-3}, and ~0.13 and 0.2 g m^{-3}, respectively, for summer and winter. The overestimation of Z_{top} will result in underestimation of LWC and N. If 200–300 m is subtracted from Z_{top}, the values of LWC and N will increase by about 30% during the summer and the summer mode value of N may rise to 50–100 cm^{-3}. However, it cannot change the seasonal variation patterns, it only reduces their winter-summer differences. Therefore, it would be necessary to investigate the seasonal variations of air mass back trajectories and aerosol properties over the ARM SGP site during the same time period as this study. That effort is beyond the scope of this paper.

Even though the aerosol properties vary seasonally, they may or may not be directly related to the seasonal variations in cloud properties. Sheridan et al. (2001) showed the monthly statistics for ground-based measurements of aerosol properties at the ARM SGP site for the 4-yr time period of 1997–2000. The maxima in aerosol concentration (~800 cm^{-3}) measured by Optical Particle Counter (OPC; diameter >0.1 μm) and aerosol total scattering coefficient (60 Mm^{-1}) occurred during August, while the condensation nuclei concentrations (CN) showed a dip (~5000 cm^{-3}) during June–August. Direct comparison between the monthly variations of aerosol properties from Sheridan et al. (2001) and the cloud properties in this study is not possible because the aerosol measurements represent all time periods. To effect a comparison, the aerosol statistics would have to include only the subset of measurements that correspond to the time periods when the cloud properties are available and must meet the following two conditions: 1) the atmosphere is well-mixed and 2) the updraft velocity is larger than 0 m s^{-1} so that the surface-based measurements of aerosols are related to those in the clouds (Delene et al. 2004).

d. A new conceptual model of midlatitude continental low clouds

Based on aircraft in situ measurements, Paluch and Lenschow (1991) developed a conceptual model of the life cycle of a marine stratus layer in the midlatitudes. It starts initially as a thin, homogenous layer, then grows and becomes patchy with time and produces precipitation. This stage is followed by the formation of small cumuli below and eventually disintegrates, leaving a field of cumuli behind. Del Genio and Wolf (2000) explained and discussed, in detail, the similarities and differences between marine and continental cloudy boundary layer, and concluded that the formation, maintenance, and dissipation processes of marine boundary layer clouds can be mostly applied to continental boundary layer clouds. Over the water, the moisture comes directly from the surface, which also maintains a relatively stable temperature throughout the day. The cloud layer undergoes a coupling and decoupling with the surface air over the diurnal cycle. Over midlatitude land areas, the water vapor is typically advected into the region with an air mass except when the surface is moist. The stratus is often formed as part of a cyclonic system. It is not surprising then that the moisture and cloud layer over the SCF can be decoupled from the surface.

Another difference lies in the fast thermal response time of the land surface. When the surface is moist, the small amount of solar radiation that penetrates through the cloud can be converted almost immediately into sensible and latent heat providing moisture directly to the cloud layer when not blocked by a strong inversion. In the coupled cases, therefore, the cloud layer would grow in the morning in opposition to the solar heating of cloud layer, which tends to destroy the cloud in marine areas during the late morning. Generating local convection to have enough turbulence is critical for forming continental low clouds as discussed by DW00. Thus, the cloud coverage can increase during the morning and be maintained until shortly after noon when the entire cloud layer is lifted (Figs. 10a, b) due to the increased LCL as discussed by DW00. During the afternoon, the cloud layer starts to disintegrate because of mixing at the top of the cloud layer and strong solar heating that makes the air parcel buoyant enough to break through the cloud-top inversion layer to form cumulus that is rapidly dissipated. Finally the low-level and overcast continental cloud layer is either dissipated or broken in the late afternoon (~1900 LT). Therefore, a new conceptual model of midlatitude continental low clouds at the SCF has been developed from this study. The low stratus cloud amount monotonically increases from midnight to early morning (0930 LT), and remains at a maximum until around local noon, then declines until 1930 LT when it levels off for the remainder of the night. In the morning the stratus cloud layer is low, warm, and thick with less LWC, while in the afternoon it is high, cold, and thin with more LWC.

7. Concluding remarks

This first part of a series of papers describing the climatological low cloud properties at the ARM SCF documents the most comprehensive dataset on continental low cloud macrophysical, microphysical, and radiative properties to date. The statistics of cloud properties between daytime and nighttime are very similar to each other and the average values are comparable to the surface-based climatology—at least, in relative terms. These results confirm part of an earlier study using ARM SCF data, but also found some differences that can be attributed to the availability of cloud radar data, which are invaluable in estimating cloud-top heights. This difference is the presence of a seasonal cycle in cloud thickness and liquid water content. The former has a summer maximum, while the latter has a winter maximum. The result is that the number density of cloud droplets is at a minimum during summer when aerosol concentrations are greatest. This finding needs further investigation.

The results are based only on measurements taken from January 1997 to December 2002 at the ARM SCF. No attempt was made to give an exhaustive climatology of the midlatitude continental low clouds as a whole; rather, the emphasis was to provide fundamental statistical information on the seasonal, monthly, and diurnal cycles of low clouds at the ARM SCF that should be useful for validation of satellite-derived cloud statistics and for improving and developing parameterizations of stratus over land in mesoscale models and in GCMs. Future installments of this series will report on other types of clouds using the longest times series of measurements available at the ARM SCF.

Acknowledgments. This research was supported by the Office of Biological and Environmental Research of the U.S. Department of Energy under Interagency Agreement No. DE-AI02-97ER62341 as part of the Atmospheric Radiation Measurement (ARM) Program. During this study, authors were also partially supported by NASA CERES project and University of North Dakota Faculty Seed Funding. Special thanks to. S. Benson and G. Mace at University of Utah for providing pre-processed ARM data, and to Dr. Del Genio and two anonymous reviewers for providing insightful comments and suggestions.

REFERENCES

Ackerman, T. P., and G. M. Stokes, 2003: The Atmospheric Radiation Measurement Program. *Phys. Today,* **56,** 38–44.

Albrecht, B. A., D. A. Randall, and S. Nicholls, 1988: Observations of marine stratocumulus clouds during FIRE. *Bull. Amer. Meteor. Soc.,* **69,** 618–626.

Bretherton, C. S., and M. C. Wyant, 1997: Moisture transport, lower tropospheric stability, and decoupling of cloud-topped boundary layers. *J. Atmos. Sci.,* **54,** 148–167.

Cess, R. D., and Coauthors, 1990: Intercomparison and interpretation of climate feedback processes in 19 atmospheric general circulation models. *J. Geophys. Res.,* **95,** 16 601–16 615.

——, and Coauthors, 1996: Cloud feedback in atmospheric general circulation models: An update. *J. Geophys. Res.,* **101,** 12 791–12 794.

Clothiaux, E. E., T. P. Ackerman, G. G. Mace, K. P. Moran, R. T. Marchand, M. A. Miller, and B. E. Martner, 2000: Objective determination of cloud heights and radar reflectivities using a combination of active remote sensors at the Atmospheric Radiation Measurement Program Cloud and Radiation Test Bed (ARM CART) sites. *J. Appl. Meteor.,* **39,** 645–665.

Curry, J. A., and Coauthors, 2000: FIRE Arctic Clouds Experiment. *Bull. Amer. Meteor. Soc.,* **81,** 5–29.

Delene, D. J., X. Dong, Y. Chen, M. Poellot, and J. Penner, 2004: Analysis of the aerosol–cloud interactions from aircraft, surface measurements, and cloud parcel model during the March 2000 IOP at the ARM SGP site. *Proc. 14th ARM Science Team Meeting*, Albuquerque, NM, Department of Energy. [Available online at http://www.arm.gov/publications/proceedings/conf14/index.stm.]

Del Genio, A. D., and A. B. Wolf, 2000: The temperature dependence of the liquid water path of low clouds in the southern Great Plains. *J. Climate,* **13,** 3465–3486.

——, M.-S. Yan, W. Kovari, and K. K.-W. Lo, 1996: A prognostic cloud water parameterization for global climate models. *J. Climate,* **9,** 270–304.

Dong, X., and G. G. Mace, 2003a: Profiles of low-level stratus cloud microphysics deduced from ground-based measurements. *J. Atmos. Oceanic Technol.,* **20,** 42–53.

——, and ——, 2003b: Arctic stratus cloud properties and radiative forcing derived from ground-based data collected at Barrow, Alaska. *J. Climate,* **16,** 445–461.

——, T. P. Ackerman, E. E. Clothiaux, P. Pilewskie, and Y. Han, 1997: Microphysical and radiative properties of stratiform clouds deduced from ground-based measurements. *J. Geophys. Res.,* **102,** 23 829–23 843.

——, ——, and ——, 1998: Parameterizations of microphysical and shortwave radiative properties of boundary layer stratus from ground-based measurements. *J. Geophys. Res.,* **103,** 31 681–31 693.

——, P. Minnis, T. P. Ackerman, E. E. Clothiaux, G. G. Mace, C. N. Long, and J. C. Liljegren, 2000: A 25-month database of stratus cloud properties generated from ground-based measurements at the ARM SGP site. *J. Geophys. Res.,* **105,** 4529–4538.

——, ——, G. G. Mace, W. L. Smith Jr., M. Poellot, R. Marchand, and A. Rapp, 2002: Comparison of stratus cloud properties deduced from surface, GOES, and aircraft data during the March 2000 ARM Cloud IOP. *J. Atmos. Sci.,* **59,** 3265–3284.

Garreaud, R. D., J. Rutllant, J. Quintana, J. Carrasco, and P. Minnis, 2001: CIMAR–5: A snapshot of the lower troposphere over the subtropical southeast Pacific. *Bull. Amer. Meteor. Soc.,* **82,** 2193–2208.

Han, Q., W. B. Rossow, J. Chou, and R. W. Welch, 1998: Global survey of the relationships of cloud albedo and liquid water path with droplet size using ISCCP. *J. Climate,* **11,** 1516–1528.

Houghton, J. T., Y. Ding, D. J. Griggs, M. Noguer, P. J. van der Linden, X. Dai, K. Maskell, and C. A. Johnson, Eds., 2001: *Climate Change 2001: The Scientific Basis*. Cambridge University Press, 881 pp.

Kato, S., T. P. Ackerman, E. E. Clothiaux, J. H. Mather, G. G. Mace, M. L. Wesely, F. Murcray, and J. Michalsky, 1997: Uncertainties in modeled and measured clear-sky surface shortwave irradiances. *J. Geophys. Res.*, **102,** 25 881–25 898.

Klein, S. A., and D. L. Hartmann, 1993: The seasonal cycle of low stratiform clouds. *J. Climate,* **6,** 1587–1606.

Liljegren, J. C., E. E. Clothiaux, G. G. Mace, S. Kato, and X. Dong, 2001: A new retrieval for cloud liquid water path using a ground-based microwave radiometer and measurements of cloud temperature. *J. Geophys. Res.,* **106,** 14 485–14 500.

Long, C. N., and T. P. Ackerman, 2000: Identification of clear skies from broadband pyranometer measurements and calculation of downwelling shortwave cloud effects. *J. Geophys. Res.,* **105,** 15 609–15 626.

Miles, N. L., J. Verlinde, and E. E. Clothiaux, 2000: Cloud-droplet size distributions in low-level stratiform clouds. *J. Atmos. Sci.,* **57,** 295–311.

Minnis, P., and E. F. Harrison, 1984: Diurnal variability of regional cloud and clear-sky radiative parameters derived from GOES data. Part II: November 1978 cloud distributions. *J. Climate Appl. Meteor.,* **23,** 1012–1031.

——, P. W. Heck, D. F. Young, C. W. Fairall, and J. B. Snider, 1992: Stratocumulus cloud properties derived from simultaneous satellite and island-based instrumentation during FIRE. *J. Appl. Meteor.,* **31,** 317–339.

Mitchell, J. F. B., and W. J. Ingram, 1992: Carbon dioxide and climate: Mechanisms of changes in cloud. *J. Climate,* **5,** 5–21.

Moran, K. P., B. E. Martner, M. J. Post, R. A. Kropfli, D. C. Welsh, and K. B. Widener, 1998: An unattended cloud-profiling radar for use in climate research. *Bull. Amer. Meteor. Soc.,* **79,** 443–455.

Paluch, I. R., and D. H. Lenschow, 1991: Stratiform cloud formation in the marine boundary layer. *J. Atmos. Sci.,* **48,** 2141–2158.

Randall, D., K.-M. Xu, R. J. C. Somerville, and S. Iacobellis, 1996: Single-column models and cloud ensemble models as links between observations and climate models. *J. Climate,* **9,** 1683–1697.

Sassen, K., 1991: The polarization lidar technique for cloud research: A review and current assessment. *Bull. Amer. Meteor. Soc.,* **72,** 1848–1866.

Sengupta, M., E. E. Clothiaux, T. P. Ackerman, S. Kato, and Q. Min, 2003: Importance of accurate liquid water path for estimation of solar radiation in warm boundary layer clouds: An observational study. *J. Climate,* **16,** 2997–3009.

Sheridan, P. J., D. J. Delene, and J. A. Ogren, 2001: Four years of continuous surface aerosol measurements from the Department of Energy's Atmospheric Radiation Measurement Program Southern Great Plains Cloud and Radiation Testbed site. *J. Geophys. Res.,* **106,** 20 735–20 747.

Stokes, G. M., and S. E. Schwartz, 1994: The Atmospheric Radiation Measurement (ARM) Program: Programmatic background and design of the cloud and radiation testbed. *Bull. Amer. Meteor. Soc.,* **75,** 1201–1221.

Wang, Z., and K. Sassen, 2002: Cirrus cloud microphysical property retrieval using lidar and radar measurements. Part II: Midlatitude cirrus microphysical and radiative properties. *J. Atmos. Sci.,* **59,** 2291–2302.

Warren, S. G., C. J. Hahn, J. London, R. M. Chervin, and R. L. Jenne, 1984: Atlas of simultaneous occurrence of different cloud types over land. NCAR Tech. Note NCAR/TN-241+STR, National Center for Atmospheric Research, Boulder, CO, 209 pp.

——, ——, ——, ——, and ——, 1986: Global distribution of total cloud cover and cloud type amounts over land. NCAR Tech. Note NCAR/TN-273+STR, National Center for Atmospheric Research, Boulder, CO, 229 pp.

Wetherald, R. T., and S. Manabe, 1988: Cloud feedback processes in a general circulation model. *J. Atmos. Sci.,* **45,** 1397–1415.

Wielicki, B. A., R. D. Cess, M. D. King, D. A. Randall, and E. F. Harrison, 1995: Mission to planet Earth: Role of clouds and radiation in climate. *Bull. Amer. Meteor. Soc.,* **76,** 2125–2153.